NOTES AND CORRESPONDENCE

On the Energy Analysis of the Two-Layer Frontal Model

CARLOS R. MECHOSO AND DOUGLAS M. SINTON

Department of Atmospheric Sciences, University of California, Los Angeles 90024

3 January 1983 and 12 April 1983

ABSTRACT

The energy analysis of the two-layer frontal model of Kotschin (1932) and Orlanski (1968) is reformulated. The new formulation is based on separating the contributions to the eddy kinetic energy of the unstable waves by the changes in 1) the difference in relative momentum between the layers (multiplied by the shear), and in 2) the available potential energy. Such a separation results in a clear characterization of the instabilities, particularly near the Rayleigh, Helmholtz and baroclinic instability limits. The mean meridional circulation induced by the unstable waves is analyzed.

1. Introduction

Kotschin (1932) and Orlanski (1968) analyzed the unstable wave solutions of the linearized version of a shallow-water system of equations for two layers of fluid on an f plane with the layer interface intersecting rigid horizontal upper and lower boundaries and with constant velocity U_i in each layer (see Fig. 1). Solutions considered are of the form

$$f(y) \times \exp[i(kx + \sigma t)],$$

where x and y are the horizontal coordinates along and across the front, respectively, t is time, k the wavenumber of the perturbation, and σ its frequency. The Richardson and Rossby numbers are defined by $\mathrm{Ri} = gH(\rho_1 - \rho_2)/(\bar{\rho}U_T^2)$ and $\mathrm{Ro} = kU_T/(2f)$, respectively, where $U_T = U_2 - U_1$, $\bar{\rho}$ is the mean density of the fluid, and g the acceleration of gravity. Hence, according to Margules formula, the slope of the interface is $H/L = Hf/(\mathrm{Ri}U_T)$. Orlanski (1968; hereafter called IFW) determined the value of τ, expressed by

$$\tau = \frac{\sigma k^{-1} + \tfrac{1}{2}(U_1 + U_2)}{\tfrac{1}{2}U_T}, \tag{1}$$

for unstable perturbations in the region $0 \leqslant \mathrm{Ro} \leqslant 3$, $0 \leqslant \mathrm{Ri} \leqslant 5$. Fig. 10 in IFW is a plot of $|\tau_i|$ as a function of Ri and Ro. The resulting surface is divided into four distinct regions, labeled in IFW as surfaces (R), (H), (E) and (B). This nomenclature conforms to the fact that, for certain limiting cases in the (Ro, Ri) parameter space, the instability problem reduces to a classical one for which the energetics is known. Surface (R) is the only one that exists for $\mathrm{Ri} \ll 1$, where the instabilities may be expected to be similar to those for $\mathrm{Ri} = 0$, in which case the interface is vertical and the problem reduces to one of the cases of the instability of parallel flows described by Rayleigh. Surface (H) is the only one that exists for $\mathrm{Ro} \gg 1$ and $\mathrm{Ri} \neq 0$, where the instabilities may be expected to be similar to those for stratified shear flows with a horizontal interface described by Helmholtz. Surface (E) is the only one that exists exclusively for small Ro and large enough Ri, where the instabilities may be expected to be similar to those described with the quasi-geostrophic formulation. Surface (B) results from the juxtaposition of (R) and (E), as explained later.

The energy block diagram in IFW is reproduced in Fig. 2. (The reader is referred to that paper for notation and derivations.) The participating terms are:

$$K_M = \int_{-\infty}^{\infty} \bar{\rho}[(H - \bar{h})U_2U_2'' - \tfrac{1}{2}U_2^2h'' + \bar{h}U_1U_1'' + \tfrac{1}{2}U_1^2h'']dy, \tag{2}$$

$$P_M = \int_{-\infty}^{\infty} (\rho_1 - \rho_2)g\bar{h}h''dy, \tag{3}$$

$$K_E = \int_{-\infty}^{\infty} \tfrac{1}{2}\bar{\rho}[\bar{h}(\langle u_1'^2\rangle + \langle v_1'^2\rangle) + (H - \bar{h})(\langle u_2'^2\rangle + \langle v_2'^2\rangle)]dy, \tag{4}$$

$$K_I = \int_{-\infty}^{\infty} \bar{\rho}[U_1\langle h'u_1'\rangle - U_2\langle h'u_2'\rangle]dy, \tag{5}$$

$$P_E = \int_{-\infty}^{\infty} \tfrac{1}{2}(\rho_1 - \rho_2)g\langle h'^2\rangle dy, \tag{6}$$

$$W_1 = \int_{-\infty}^{\infty} \bar{\rho}\left[\frac{d\bar{h}}{dy}(U_1\langle u_1'v_1'\rangle - U_2\langle u_2'v_2'\rangle) - (U_1\langle u_1'w_1'\rangle - U_2\langle u_2'w_2'\rangle) + \tfrac{1}{2}f\bar{U}(\langle h'v_2'\rangle - \langle h'v_1'\rangle) + (H - \bar{h})V_2'' + \bar{h}V_1'')]dy, \tag{7}$$

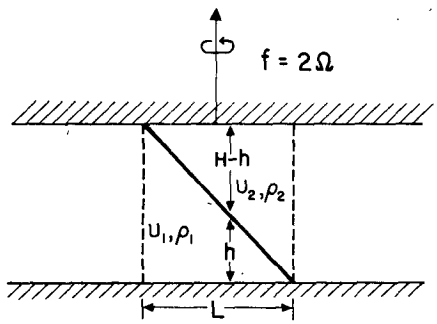

FIG. 1. Schematic of the two-layer frontal model.

$$W_2 = -\int_{-\infty}^{\infty} \tfrac{1}{2} f \bar{\rho} U_T[(H - \bar{h})V_2'' - \bar{h}V_1'']dy, \tag{8}$$

$$W_3 = -\int_{-\infty}^{\infty} \tfrac{1}{2} f \bar{\rho} U_T[\langle h'v_1' \rangle + \langle h'v_2' \rangle]dy, \tag{9}$$

$$W_4 = \int_{-\infty}^{\infty} U_T \left\langle p_2' \frac{\partial h'}{\partial x} \right\rangle dy, \tag{10}$$

$$W_5 = -\int_{-\infty}^{\infty} [(H - \bar{h})\langle \mathbf{v}_2' \cdot \nabla p_2' \rangle + \bar{h}\langle \mathbf{v}_1' \cdot \nabla p_1' \rangle]dy. \tag{11}$$

Here $\bar{h}$ is the basic interface height, p_i the pressure in the ith layer, $\mathbf{v}_i = (u_i, v_i)$ is the horizontal velocity and w_i the vertical velocity. First- and second-order perturbation fields are identified with primes and double primes, respectively. Angle braces imply average in x. Second-order perturbations are independent of x. Note that some of the original expressions for the energy conversions in IFW have been modified to make W_2 and W_3 independent of $\bar{U} = (U_1 + U_2)/2$. The conversions between eddy available potential and eddy kinetic energies can be written as

$$W_5 + W_3 - W_4 = -\int_{-\infty}^{\infty} \tfrac{1}{2}(\rho_1 - \rho_2)g[\langle h'w_1' \rangle + \langle h'w_2' \rangle]dy. \tag{12}$$

The perturbation interface height in (6), (9), (10) and (12) is dynamically analogous to the temperature field in the continuous model. The conversion between zonal kinetic and zonal available potential energies is given by the mean meridional circulation. This will be referred to as direct (indirect) when $W_2 < 0 (W_2 > 0)$.

Several difficulties are found when attempting to use such an energy formulation for characterizing the instabilities in particular cases. First, $W_1 = 0$ in the Rayleigh, Helmholtz and quasi-geostrophic limits. In the first two limits there is no source of energy for the perturbation other than at the interface. In the quasi-geostrophic limit, W_1 is relegated to a higher order in the perturbation expansion. Consequently, from the energetics viewpoint, no distinction between the classical limiting cases can be established from this term. Second, dK_M/dt, dK_I/dt and W_1 remain dependent on $\bar{U}$ in general. Third, the sign of $d(K_E + K_I)/dt$ is not known *a priori* because dK_I/dt is not necessarily positive, and a change in its sign is not easily interpreted.

In the next section we propose a modification and extension of this energy analysis that makes clearer the characterization of the instabilities in the two-layer frontal model.

2. The proposed energy analysis

We consider for the moment that U_i and the slope of the interface depend on y. In this case

$$\frac{d}{dt} K_M = W_1 - W_2 - W_6, \tag{13}$$

$$\frac{d}{dt} K_E = W_5 + W_6, \tag{14}$$

where W_6 is the energy conversion associated with the shear of the basic flow in each layer:

$$W_6 = -\int_{-\infty}^{\infty} \bar{\rho}\left[(H - \bar{h})\langle u_2'v_2' \rangle \frac{dU_2}{dy} + \bar{h}\langle u_1'v_1' \rangle \frac{dU_1}{dy}\right]dy. \tag{15}$$

The second-order relative momentum at one point in each layer is

$$m_1 = \bar{\rho}[\bar{h}U_1'' + U_1h'' + \langle h'u_1' \rangle], \tag{16}$$

$$m_2 = \bar{\rho}[(H - \bar{h})U_2'' - U_2h'' - \langle h'u_2' \rangle]. \tag{17}$$

It is straightforward to show that

$$\frac{d}{dt}(K_M + K_I) = \frac{d}{dt}\int_{-\infty}^{\infty} [U_1m_1 + U_2m_2]dy + \frac{d}{dt}\int_{-\infty}^{\infty} \tfrac{1}{2}\bar{\rho}(U_2^2 - U_1^2)h''dy. \tag{18}$$

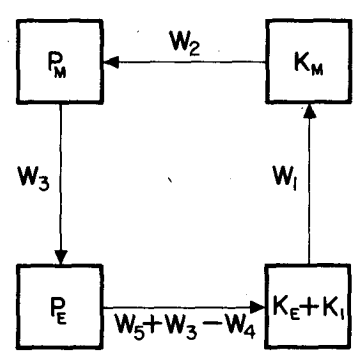

FIG. 2. The energy block diagram in Orlanski (1968).

Therefore, $d(K_M + K_I)/dt$ reflects the second-order changes in the relative momentum of each layer and in the position of the interface. Further, it can be shown that

$$\frac{d}{dt}\int_{-\infty}^{\infty}[U_1 m_1 + U_2 m_2]dy = W_3 - W_2 - W_4 - W_6 - C, \quad (19)$$

$$\frac{d}{dt}\int_{-\infty}^{\infty} \tfrac{1}{2}\bar{\rho}(U_2^2 - U_1^2)h''dy = C, \quad (20)$$

where C is given by

$$C = \int_{-\infty}^{\infty} \tfrac{1}{2}\bar{\rho}\left\{[\bar{h}V_1'' + \langle h'v_1'\rangle]\frac{d}{dy}U_1^2 + [(H-\bar{h})V_2'' - \langle h'v_2'\rangle]\frac{d}{dy}U_2^2\right\}. \quad (21)$$

We now come back to the case U_i = constant, where $W_6 = C = 0$. In this case we can take $U_2 = U_T/2$, $U_1 = -U_T/2$, obtaining

$$\frac{d}{dt}(K_M + K_I) = \tfrac{1}{2}U_T\frac{d}{dt}(M_2 - M_1), \quad (22)$$

where M_1 and M_2 are the relative momentum of each layer

$$M_1 = \int_{-\infty}^{\infty} m_1 dy, \quad (23)$$

$$M_2 = \int_{-\infty}^{\infty} m_2 dy. \quad (24)$$

It follows that $d(K_M + K_I)/dt < 0$ for an unstable wave which reduces the magnitude of the difference in relative momentum between the layers. A new version of the energy block diagram for the U_i = constant case whose design was motivated by the above considerations is in Fig. 3. W_1 is no longer present and all the energy conversions W_i are independent of $\bar{U}$. The conversion $W_4 - W_3$ can be easily interpreted after obtaining, with a few manipulations,

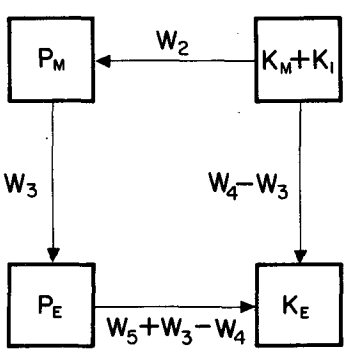

FIG. 3. The proposed energy block diagram.

$$W_4 - W_3 = -\int_{-\infty}^{\infty}\left[(H-\bar{h})\frac{\partial}{\partial y}\langle v_2'p_2'\rangle + \bar{h}\frac{\partial}{\partial y}\langle v_1'p_1'\rangle - \tfrac{1}{2}\langle(w_2' - w_1')(p_1' + p_2')\rangle\right]dy. \quad (25)$$

Thus it is the wave energy flux convergence.

In the Helmholtz limit $f = 0$ gives $W_2 = W_3 = 0$. Furthermore, $W_5 - W_4 < 0$ for growing waves. In the quasi-geostrophic limit the horizontal velocities in W_3 must be replaced by their geostrophic components giving $W_3 - W_4 = 0$ and $W_5 + W_3 - W_4 > 0$. Furthermore, $W_2 > 0$ (indirect mean meridional circulation) for this case.

The Rayleigh limit requires more elaboration. In this case, the flow in each layer is two-dimensional and non-divergent: $P_M = 0$, $P_E = 0$ and $W_5 + W_3 - W_4 = 0$ when $\rho_1 = \rho_2$, according to (3), (6) and (12), respectively. For a vertical front h' represents the *horizontal* displacement of the interface. The dynamic and kinematic boundary conditions [see (4.4), (4.5) and (4.6) in IFW] give $W_2 = 0$, and

$$W_3 = \int_{-\infty}^{\infty} f\bar{\rho}U_T\frac{d}{dt}\langle h'^2\rangle dy. \quad (26)$$

In this case, the expressions $dP_M/dt = -W_3$, and $dP_E/dt = W_3$ can be formally interpreted as definitions of P_M and P_E that replace (3) and (6), respectively, and not as equations for the energy of the system. For unstable perturbations in this limit $W_4 - W_3 > 0$.

The above considerations suggest a graphical representation to describe the energetics of the unstable waves. Such a representation is based on the direction of the unit vector **Z**, defined by

$$\mathbf{Z} = \frac{[(W_4 - W_3)\mathbf{i} + (W_5 + W_3 - W_4)\mathbf{j}]}{[(W_4 - W_3)^2 + (W_5 + W_3 - W_4)^2]^{1/2}}, \quad (27)$$

where **i** and **j** are orthogonal unit vectors. **Z** becomes **i** in the Rayleigh limit and **j** in the quasi-geostrophic limit. In the Helmholtz limit, $\mathbf{Z}\cdot\mathbf{i} > 0$ and $\mathbf{Z}\cdot\mathbf{j} < 0$, placing **Z** in the fourth quadrant.

3. Results and discussion

Fig. 4 shows $|\tau_i|$ as a function of Ro for Ri = 0.5, 2.1, 6.5 and 10. They were computed by using the same numerical method as in IFW with 200 points in the frontal region. The arrows represent **Z**, defined in (27), at each point with **i** pointing to the right and **j** pointing upwards. Solid arrows are for $W_2 > 0$, whereas dashed arrows are for $W_2 < 0$. Surfaces are labelled as in IFW. Each point on the (R), (E), and (E_1) surfaces represents one growing mode whose phase speed is $\bar{U}$, i.e., such that $|\tau_r| = 0$, while each point on the (H) and (B) surfaces represents two growing modes whose phase speeds relative to $\bar{U}$ are equal in magnitude but opposite in sign, i.e., with the same $|\tau_r|$. One of these modes has its maximum amplitude

in the upper layer, whereas the other mode has its maximum amplitude in the lower layer.

For Ri = 0.5, Fig. 4a reveals that **Z** for surface (R) is near the Rayleigh limit of **i** for small Ro, rotating counterclockwise as Ro increases. On the other hand, **Z** for (H) rotates clockwise with increasing Ro, until, for large Ro, it is in the fourth quadrant or Helmholtz limit. Note that a counterclockwise (clockwise) rotation of **Z** implies that the perturbations receive a decreasing (increasing) contribution to their kinetic energy through the reduction of the relative momentum difference between the layers. For Ro $\gtrsim$ 1.2, $W_2 < 0$ indicating that the mean meridional circulation induced by the unstable waves is a direct one. (We will discuss this point later in this section.) The largest values of $|W_2|$ (normalized by $|W_4|$) occur in the neighborhood of $|\tau_i| = 0$.

For Ri = 2.1, Fig. 4b reveals that surface (E) has appeared. For small Ro, **Z** for this surface is close to the quasi-geostrophic limit of **j**, while **Z** for surface (R) is near the Rayleigh limit of **i**. W_2 for (E) modes is larger than for corresponding (R) modes. As Ro increases, **Z** for (E) rotates clockwise toward **i**, while **Z** for (R) rotates counterclockwise toward **j**. Thus the **Z** vectors for (R) and (E) become more aligned until they coincide at Ro $\approx$ 0.4. For 0.4 $\leqslant$ Ro $\leqslant$ 0.48 there are two growing modes with the same growth rate but different phase speeds, and surfaces (R) and (E) juxtapose forming the (B) surface. At Ro $\gtrsim$ 0.48 there is one growing (R) mode and the (R) surface continues with **Z** resuming its counterclockwise rotation with increasing Ro. At Ro $\approx$ 1.0, **Z** rotates through **j**. However, as opposed to the case in the quasi-geostrophic limit, the induced mean meridional circulation here is direct ($W_2 < 0$). Note that with $W_2 < 0$ and $W_4 - W_3 < 0$ (i.e., **Z** in the second quadrant), the difference in relative momentum between the layers is actually increasing according to (22) and Fig. 3. As before, $W_2 < 0$ for larger Ro with the largest values for $|W_2|$ occurring in the neighborhood of $|\tau_i| = 0$.

For Ri = 6.5, Fig. 4c reveals that surface (E_1) has appeared; (E_1) modes have a finer structure in the y-direction than (E) modes. All the **Z** vectors for this surface maintain a similar orientation near the quasi-geostrophic limit of **j** and in the second quadrant ($W_4 - W_3 < 0$). For very small Ro, **Z** vectors for surfaces (R) and (E) are rotated counterclockwise of their corresponding counterparts in Fig. 4b. In particular, the vectors for (R), while remaining in the first quadrant, are closer to **j** than to **i**, announcing the disappearance of the (R) modes for larger Ri. As

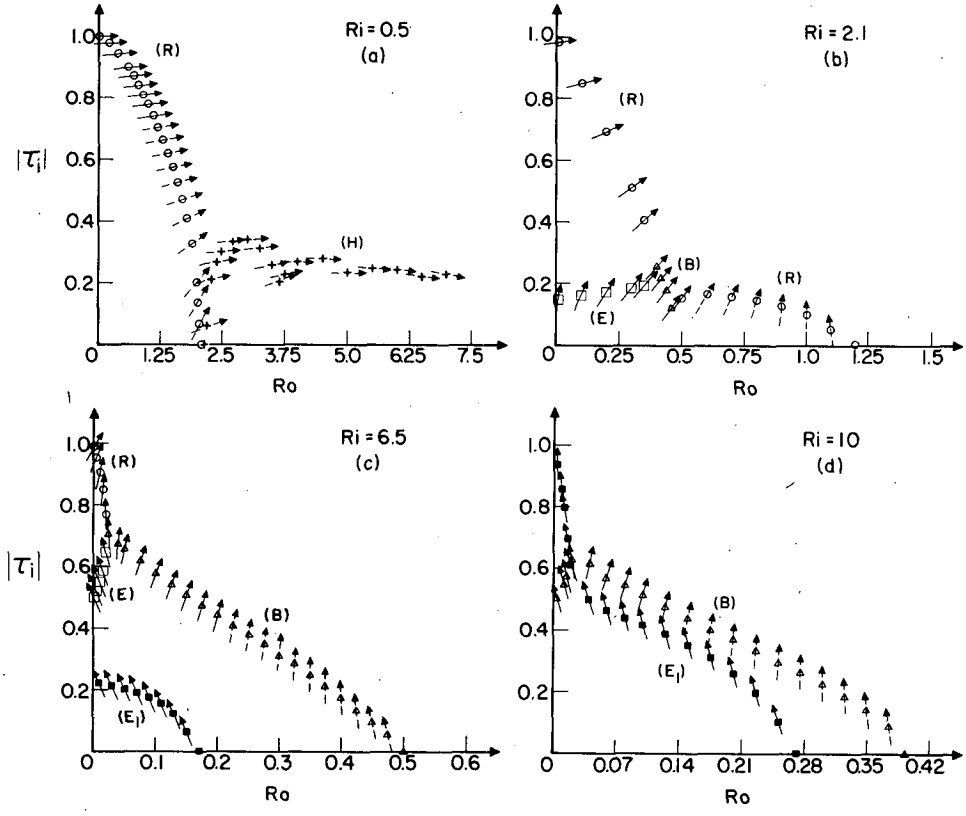

FIG. 4. $|\tau_i|$ as a function of Ro for (a) Ri = 0.5, (b) Ri = 2.1, (c) Ri = 6.5 and (d) Ri = 10. The arrows represent **Z** as defined in the text.

Ro increases, **Z** vectors for (R) and (E) rotate counterclockwise and clockwise, respectively, as in Fig. 4b. The **Z** vectors for surface (B) in Fig. 4c resemble those for surfaces (B) and (R) at larger Ro in Fig. 4b.

The presence of (R), (B), (E) and (E_1) modes for Ri = 6.5 suggests that this is a convenient place to discuss the mean meridional circulation induced by unstable modes. For simplicity in the notation we define

$$V_1 = \bar{h}V_1'', \tag{28}$$

$$V_2 = (H - \bar{h})V_2''. \tag{29}$$

With these definitions, W_2 defined by (8) becomes

$$W_2 = -\int_{-\infty}^{\infty} \tfrac{1}{2} f \bar{\rho} U_T (V_2 - V_1) dy. \tag{30}$$

The conversion W_2 can then be evaluated after solving the following system of equations which are obtained after manipulations with the second-order relations

$$g(\rho_1 - \rho_2)\bar{h}(H - \bar{h})\frac{\partial^2 V_2}{\partial y^2} + \bar{\rho}(4\sigma_i^2 + f^2) \times [(H - \bar{h})V_1 - \bar{h}V_2] = F + G + Q_2, \tag{31}$$

$$g(\rho_1 - \rho_2)\bar{h}(H - \bar{h})\frac{\partial^2 V_1}{\partial y^2} - \bar{\rho}(4\sigma_i^2 + f^2) \times [(H - \bar{h})V_1 - \bar{h}V_2] = -F - G - Q_1, \tag{32}$$

where the forcing terms are given by

$$F = -\bar{\rho} f \bar{h}(H - \bar{h})\left(\frac{\partial}{\partial y}\langle u_2' v_2' \rangle - \frac{\langle u_2' w_2' \rangle}{H - \bar{h}} - \frac{\partial}{\partial y}\langle u_1' v_1' \rangle - \frac{\langle u_1' w_1' \rangle}{\bar{h}}\right), \tag{33}$$

$$G = -2\bar{\rho}\sigma_i \bar{h}(H - \bar{h})\left(\frac{\partial}{\partial y}\langle v_2' v_2' \rangle - \frac{\langle v_2' w_2' \rangle}{H - \bar{h}} - \frac{\partial}{\partial y}\langle v_1' v_1' \rangle - \frac{\langle v_1' w_1' \rangle}{\bar{h}}\right), \tag{34}$$

$$Q_1 = g(\rho_1 - \rho_2)\bar{h}(H - \bar{h})\frac{\partial^2}{\partial y^2}\langle h' v_1' \rangle, \tag{35}$$

$$Q_2 = g(\rho_1 - \rho_2)\bar{h}(H - \bar{h})\frac{\partial^2}{\partial y^2}\langle h' v_2' \rangle. \tag{36}$$

Boundary conditions for this system at the boundaries of the frontal region are

$$V_1 = 0, \quad V_2 = \langle h' v_2' \rangle - \langle h' v_1' \rangle \quad \text{at} \quad y = 0, \tag{37}$$

$$V_1 = \langle h' v_2' \rangle - \langle h' v_1' \rangle, \quad V_2 = 0 \quad \text{at} \quad y = L, \tag{38}$$

after taking into account (28), (29) and expression (B.20) in IFW which is obtained from the second-order continuity equations for both layers.

Note that the forcing functions F and G represent Reynolds stresses while Q_1 and Q_2 represent the meridional variation of the meridional interface height flux convergence. These forcing functions are analogous to the adiabatic version of those that in Kuo (1956) represent the net effect of the convergence of the eddy transfer of zonal and meridional momentum and the convergence of eddy heat-transfer.

The linearity of the system allows the separation of the solution in three components, each of them forced by each one of the forcing functions (33)–(36), namely,

$$V_1 = V_{1F} + V_{1G} + V_{1Q}, \tag{39}$$

$$V_2 = V_{2F} + V_{2G} + V_{2Q}. \tag{40}$$

The boundary conditions for the components are

$$V_{1F} = V_{1G} = V_{1Q} = V_{2F} = V_{2G} = 0,$$
$$V_{2Q} = \langle h' v_2' \rangle - \langle h' v_1' \rangle \quad \text{at} \quad y = 0, \tag{41}$$
$$V_{1Q} = \langle h' v_2' \rangle - \langle h' v_1' \rangle,$$

$$V_{1F} = V_{1G} = V_{2F} = V_{2G} = V_{2Q} = 0 \quad \text{at} \quad y = L. \tag{42}$$

Solid lines in Fig. 5 show the value of W_2 normalized by W_4 (which is the net conversion from zonal to eddy energies) as a function of Ro for Ri = 6.5. W_2 increases with increasing Ro for (R) modes and decreases for (B), (E) and (E_1) modes. A consistent feature for all modes is that the Reynolds stress terms (dotted and dashed-dotted lines for W_2 forced by F and G, respectively) contribute to induce an indirect mean meridional circulation, whereas the interface height transport terms (dashed lines) induce a direct one. Reynolds stresses predominate at smaller Ro for all modes. The interface height transport terms predominate at larger Ro for (B) modes, and for (R) modes when they exist for large Ro (see Fig. 4). Note that, except for (B) modes, the contribution to W_2 by the Reynolds stresses associated with the across-front velocity component is negligible [the analogous term was neglected in Kuo (1956)].

For Ri = 10, Fig. 4d reveals that surface (R) is undetectable as (B) now extends to the vicinity of Ro = 0 (Duffy, 1976), where **Z** vectors are similar to those for (E) in Fig. 4c. The vectors for (B) rotate clockwise into the first quadrant for smaller Ro while they rotate counterclockwise for larger Ro, much in agreement with those for (B) in Fig. 4c. The vectors for (E_1) are close to the quasi-geostrophic limit of **j** for very small Ro. As before, $W_2 > 0$ for all (E_1) modes. $W_2 < 0$ for all (B) modes with Ro $\gtrsim 0.15$, the largest $|W_2|$ occurring in the neighborhood of $|\tau_i| = 0$.

There is an important difference between the structures of (B) modes and (E_1) modes for the same Ro. The maximum amplitudes of (B) modes occur at the intersection of the interface with the upper and/or

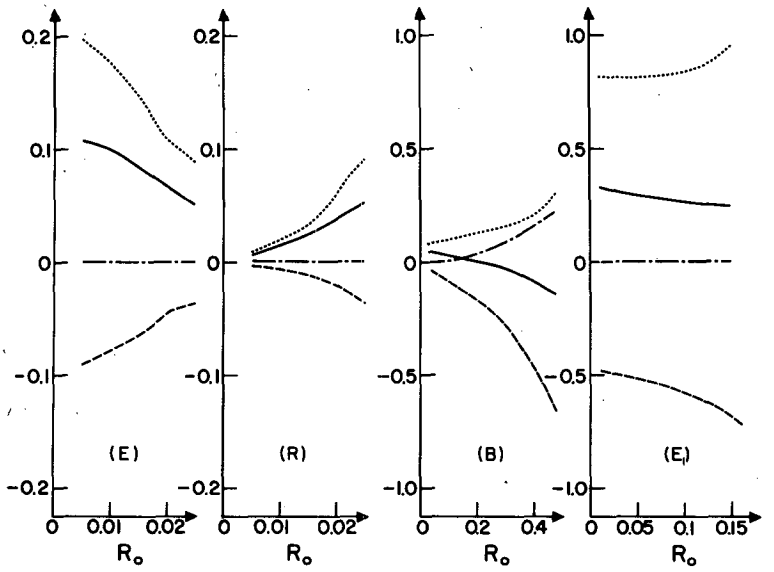

FIG. 5. W_2/W_4 for Ri = 6.5 (solid lines). Contributions of the Reynolds stress terms are indicated by dotted and dashed-dotted lines, while contributions of the interface height transport terms are indicated by dashed lines.

lower boundary where the flow is fundamentally non-geostrophic. On the other hand, amplitudes of (E_1) modes have pronounced secondary maxima well inside the frontal region where the flow is close to quasi-geostrophic for small Ro. Therefore, (E_1) modes are closer to being quasi-geostrophic than (B) modes.

In summary, we find that the proposed energy analysis makes clearer the characterization of the instabilities in the two-layer frontal model. The results support the characterization of the instabilities given by IFW in limiting cases of the region explored in that study. Specifically, Rayleigh, Helmholtz, and quasi-geostrophic instability mechanisms are shown to prevail as (R), (H), (E), and (E_1) modes are analyzed near their respective limits. Far from those limits, the characteristics of the modes are less well defined. We find that (R) modes disappear for large enough Ri. Our calculations indicate that the mean meridional circulation induced by the unstable (E) and (E_1) modes is always indirect, whereas that induced by the (R) and (B) modes switches from indirect to direct as the length scale of the perturbation decreases.

Acknowledgments. The authors are grateful to Professors I. Orlanski, A. Arakawa and S. V. Venkateswaran for useful comments. Mrs. B. Gola typed the manuscript and Ms. M. Archie drafted the figures. This research was supported by the National Science Foundation under Grant ATM-78-01922.

REFERENCES

Duffy, D. G., 1976: The application of the semi-geostrophic equations to the frontal instability problem. *J. Atmos. Sci.*, **33**, 2322–2337.

Kotschin, N., 1932: Uber die Stabilitat von Margulesschen Diskontinuitatsflachen. *Beitr. Phys. Atmos.*, **18**, 129–164.

Kuo, H.-L., 1956: Forced and free meridional circulations in the atmosphere. *J. Meteor.*, **13**, 561–568.

Orlanski, I., 1968: Instability of frontal waves. *J. Atmos. Sci.*, **25**, 178–200.